Title
The growth and stress vs. strain characterization of the silver solid solution phase with indium

Authors
Huo, Yongjun
Lee, Chin C

Publication Date
2016-03-01

DOI
10.1016/j.jallcom.2015.11.212

Peer reviewed

Journal of Alloys and Compounds 661 (2016) 372–379

Contents lists available at ScienceDirect

Journal of Alloys and Compounds

journal homepage: http://www.elsevier.com/locate/jalcom

The growth and stress vs. strain characterization of the silver solid solution phase with indium

Yongjun Huo [a, b, *], Chin C. Lee [a, b]

[a] Electrical Engineering and Computer Science, University of California, Irvine, CA 92697-2660, USA
[b] Materials and Manufacturing Technology, University of California, Irvine, CA 92697-2660, USA

ARTICLE INFO

Article history:
Received 6 October 2015
Received in revised form
25 November 2015
Accepted 27 November 2015
Available online 2 December 2015

Keywords:
Silver–indium solid solution
Ingots growth
Stress vs. strain characterization
Mechanical properties
Fractography

ABSTRACT

Silver solid solution phase with indium has been discovered to have great mechanical properties and anti-tarnishing property, as shown in the results of our previous study. It is important to know the stress vs. strain curve before adopting this material in industrial applications. The growth of the homogeneous silver solid solution phase with indium is first described. The X-ray diffraction (XRD) patterns and scanning electron microscope/energy dispersive X-ray spectroscopy (SEM/EDX) results are reported to verify the chemical composition of silver solid solution phase with indium samples. Based on the results, one could reversely determine the indium element composition in (Ag)–xxIn solid solution by examining the lattice constant value using XRD for unknown compositions. The preparation of ASTM tensile test samples and tensile test experimental setting are explained in details. The intrinsic mechanical material properties of silver solid solution phase with indium, i.e., characteristic stress vs. strain curves, are presented and analyzed, with pure silver stress vs. strain curve in comparison. According to the experimental results, silver solid solution phase with indium exhibits low yield strength, high ultimate tensile strength, and large elongation value before fracture, compared to pure silver. In addition, fractography of the fracture surface of the tested sample has been studied to confirm the superior ductility of silver solid solution phase with indium. These superior mechanical properties may bring silver solid solution phase with indium new applications in various industries such as electronics and brazing.

1. Introduction

The material properties of silver and its solid solution had been studied for near a century. In the early days of material and metallurgical science, the lattice constant [1] and elastic constant [2] have been measured and investigated thoroughly for silver primary solid solution, namely, silver solid solution of cadmium, indium, tin, antimony, etc. Solid solution strengthening mechanism is well-known, responsible for increasing the yield strength and hardness of metal which is the result of the interactions between dislocations and solute atoms by following mechanisms: elastic interaction, modulus interaction, stacking-fault interaction, electrical interaction, short-range order and long-range order interaction [3]. Several theoretical models have been proposed for specifically describing the solid solution strengthening mechanisms of silver or FCC crystal structure metal based solid solution [4–6]. However, the research for investigating the mechanical behaviors, especially plasticity of silver based alloy is relatively seldom and underdeveloped, which is possibly due to the fact that silver and its alloy are not major metallic material for structural engineering applications. Recently, silver based alloys have been adopted as a new alternative in interconnection applications [7,8]. Therefore, silver-based solid solution mechanical properties, especially plasticity, would be of a great interest to the electronic devices manufacturing and packaging industry since it is closely related to the manufacturability of the silver alloy based products, and the performance and reliability of electronic components during and after the process of the manufacturing. Stress–strain curve obtained in the tensile test is widely used to provide fundamental information on the strength and mechanical properties for engineering applications. Therefore, the stress–-strain curves of silver solid solutions would be very useful and important for the further research and development in this area.

Our research group has been studying the Ag–In system for almost two decades [9], and developed several important fluxless

* Corresponding author. Electrical Engineering and Computer Science, University of California, Irvine, CA 92697-2660, USA.
E-mail address: yongjunh@uci.edu (Y. Huo).

http://dx.doi.org/10.1016/j.jallcom.2015.11.212
0925-8388/

bonding technologies based on the Ag–In binary system. During the previous research, the authors have identified two major intermetallic compound, namely Ag_2In and $AgIn_2$ [10]. Recently, our research group has successfully converted almost all of those intermetallic compounds into silver–indium solid solution phase [11], which is designated as (Ag)–xxIn in this paper. The experimental results show that the properties of the bonding joint with (Ag)–xxIn phase are intriguingly great. Thus, as following research, we decided to produce (Ag)–xxIn single phase ingots with varied indium concentration to study the properties of this interesting material. The authors have recently reported the great anti-tarnishing property of silver–indium solid solution phase [12]. To the best of our knowledge, the mechanical properties and stress vs. strain curves of (Ag)–xxIn phase are not available in any scientific or engineering database. In this article, the authors would like to reveal the some details of the material in preparation, and present the characteristic stress–strain curves of silver–indium solid solution with analysis of its mechanical properties.

In the following sections, the authors would like to present the preparation and characterization of (Ag)–xxIn phase material in the polycrystalline form at two different indium compositions with further details. Secondly, the preparation of tensile test samples and the experimental setting of the tensile test are described, followed by the representative results of the tensile test, i.e., stress vs. strain curves, with analysis and discussions. In addition, SEM pictures of the morphology of fractured tensile test samples are presented, following with analysis of the fracture mode and failure mechanism. Lastly, the authors would like to share the vision in terms of the implications of mechanical properties of (Ag)–xxIn solid solution and its potential industrial utility due to its superior intrinsic mechanical behaviors under tensile stress.

2. Material preparation and characterization

In order to understand Ag–In binary system and produce the single phase (Ag)–xxIn material, it is essential to review the Ag–In binary phase diagram. As shown in silver–indium phase diagram, Fig. 1 [13], the maximum solubility of indium element in silver crystal lattice is 20 at.% at room temperature, the silver–indium solid phase with face-centered cubic (FCC) crystal structure is designated as α phase historically. In Ref. [14], the authors discovered α′ phase, which has also cubic crystal structure, at the composition of 25 at.%, and it is correspond to Ag_3In which is transformed from ζ phase at 187 °C. It is important to note that

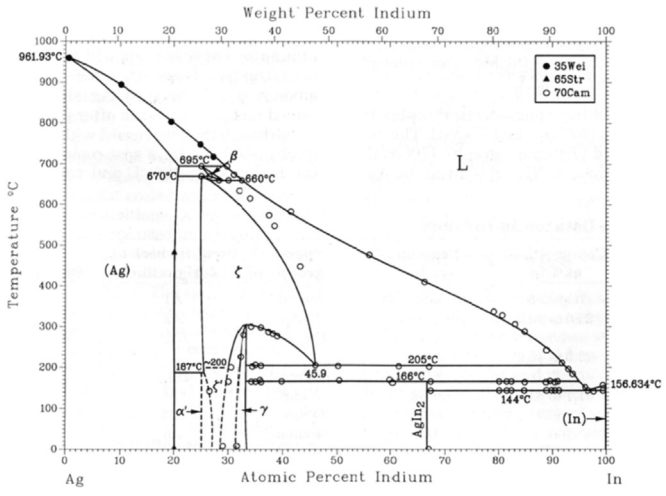

Fig. 1. Silver–indium binary phase diagram.

material composition may fluctuate from region to region, which can be caused by various mechanism of segregation effects. Therefore, it is necessary to give enough clearance to the maximum solubility boundary in order to avoid entering the mixture region of α and α′ phase in the phase diagram, thereby producing nearly homogeneous single phase silver–indium solid solution. Therefore, (Ag)–xxIn with 19 at.% indium concentration has been chosen as the primary research subject, which is designated as (Ag)–19In in this article. In addition, (Ag)–xxIn with 9.5 at.% indium concentration, which is designated as (Ag)–9.5In, has been also produced and investigated in order to observe the influence of the amount of indium element composition on the properties of (Ag)–xxIn phase. Pure silver has also been grown using the same method as the controlled group for the following experiments.

The casting method was chosen for the production of the material of the interested phase, resulting in the form of ingots. The raw materials of silver and indium shots with 99.99% purity were weighed, uniformly mixed and loaded in quartz tube with one end closed. Since the native oxide forming on the surface of silver and indium metal is negligible thin, there is no treatment required to perform before loading the raw material. While the quartz tube is being pumped by a vacuum pump, the other end of the tube is sealed by hydrogen–oxygen torch operation to form a capsule. The vacuum environment is necessary for the casting production for reducing the number of voids or common defects created by trapped air bubbles. Next, the capsule was placed into a furnace preheated at 1030 °C and stayed there for 30 min. The temperature of the furnace was then reduced gradually to room temperature in 7 days in order to obtain the homogenized single phase solid solution at different compositions. This is the preliminary process and optimization requires more time and many growth runs.

After the successful production of (Ag)–xxIn solid solution, the ingots were cut into disk samples, using slow speed diamond saw, for further chemical composition examination. X-ray diffraction (XRD) and scanning electron microscope/energy dispersive X-ray spectroscopy (SEM/EDX) were used in a combination to identify (Ag)–xxIn phase, since their functionality are complementary to each other. While SEM/EDX can provide information about specific chemical composition at local areas within its electron-beam interaction volume, a few micron meters or sub-micron range depending on the electron beam energy and atomic number of the material under examination, XRD is capable of interpreting the crystallography nature of the material by generalizing data generated from macroscopic regions of the samples, thereby identifying the phases of the unknown material precisely and accurately. Before material characterization, the disk samples were prepared by polishing process in the sequence of 120/240/800/1200 grits, using silicon carbide abrasive papers.

FEI/Philips XL-30 FEG SEM in the Laboratory for Electron and X-ray Instrumentation (LEXI) was used for the SEM/EDX examination. Several local areas of the disk samples were randomly chosen to be examined by SEM/EDX. For example, as shown in Fig. 2, nine points of interests have been examined by SEM/EDX at 1000× magnification for each (Ag)–9.5In and (Ag)–19In disk samples respectively, and the results of chemical compositions are listed in Table 1.

According to the SEM/EDX machine setting, the errors of compositions are ±0.88 at.% and ±0.54 at.% for Ag and In respectively. Therefore, the variation of chemical compositions for the data shown in Table 1 is within the range of the error that due to the uncertainty of the SEM/EDX detector, expect for a few points deviation from the intended value.

After determination of the chemical composition, Rigaku SmartLab X-ray diffractometer in LEXI was used for further phase identification, using Bragg-Brentano (BB) operation mode with θ-θ diffractometer setting. During XRD examination, the disk sample

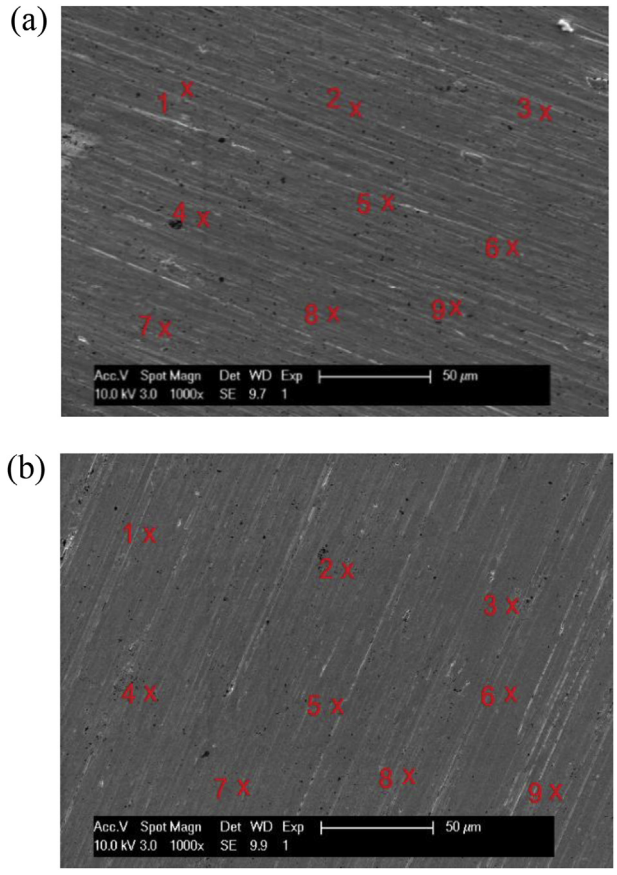

Fig. 2. (a) (Ag)–9.5In disk SEM/EDX tested region, (b) (Ag)–19In disk SEM/EDX tested region.

Table 1
SEM/EDX results of chemical compositions for (Ag)–9.5In and (Ag)–19In disk in the tested region.

	(Ag)–9.5In		(Ag)–19In	
	Ag (at.%)	In (at.%)	Ag (at.%)	In (at.%)
1	90.97	9.03	81.73	18.27
2	90.92	9.08	81.43	18.57
3	91.32	8.68	81.24	18.76
4	91.23	8.77	80.61	19.39
5	92.28	7.72	82.24	17.76
6	90.01	9.99	81.54	18.46
7	90.60	9.40	81.01	18.99
8	90.91	9.09	81.39	18.61
9	90.72	9.28	80.68	19.32

remains stationary and the detector and X-ray source rotate at the same angular speed. To be more specific, the XRD measurement conditions and parameters are summarized in Table 2. The results of XRD examination for (Ag)–9.5In and (Ag)–19In disk samples are shown in Fig. 3, with pure Ag disk sample XRD result as reference. The XRD measurement data have been collected and analyzed by PDXL, an integrated powder X-ray analysis software package. The crystallography information for the silver–indium solid solution can be learned thusly from the XRD diffraction, which is listed in Table 3.

As shown Fig. 3, it is very clear that (Ag)–9.5In and (Ag)–19In resemble the crystal structure of pure silver, face-centered cubic (FCC) crystal structure, for its typical systematically peaks absence. In addition, there are no major peaks other the peaks of Ag, (Ag)–9.5In, (Ag)–19In in each XRD patterns. Therefore, it can be safely concluded that the materials in the disk samples are nearly homogeneous and polycrystalline. In Table 3, (h, k, l) is the Miller's indices with classic denotation, d is the d-spacing value for corresponding crystal plane, and a is the calculated lattice constant by using the values of each d-spacing. As results, the X-ray diffraction patterns have shifted towards left as the indium element composition increases, which is corresponding to the increasing values of lattice constants from pure Ag, (Ag)–9.5In to (Ag)–19In. The weighted average values for lattice constants are 4.094 Å, 4.126 Å, and 4.153 Å for pure Ag, (Ag)–9.5In, and (Ag)–19In respectively. The trend of increasing values for lattice constants can be explained by reviewing atomic radius for silver and indium elements. The atomic radius for indium, 167 pm, is larger than that of silver atom, 144 pm, so that if one substitutes silver atoms with indium atoms in the original FCC lattice sites, it would result in the bulge in its crystal structure, thereby increasing the values of the lattice constants as indium element composition increased. In other words, one could reversely determine the indium element composition in (Ag)–xxIn solid solution by examine the lattice constant value using XRD for unknown compositions in the future study. Even though the authors have the awareness of that the radius for silver and indium metallic ions in the metal are different from the values of their atomic radius of solo atoms, the general principle must be plausible for this analysis approach.

The SEM/EDX and XRD results shown above are representatives for disk samples' chemical composition and crystallography examination, and results in general are similar and repeatable for different examined regions, disk samples, and ingots. In conclusion, our research group has been successfully grown the nearly homogeneous and polycrystalline (Ag)–9.5In and (Ag)–19In ingots, using the casting method in a quartz capsule with vacuum pumped and specific annealing profiles within the laboratory and research facility. However, there are still some space for improvement in terms of the ingots growth procedure and annealing profile design.

3. Tensile test

After obtaining nearly homogeneous ingots of (Ag)–9.5In and (Ag)–19In, tensile test samples, conforming with American Society for Testing and Materials (ASTM) standard E8/E8M- 08 [15], were machined by electrical discharge machining (EDM) which is

Table 2
A summary of Rigaku SmartLab X-ray diffractometer measurement conditions and parameters.

X-ray source	40 kV, 44 mA	Scan speed/duration time	2.0000 deg./min.
Goniometer	None	Step width	0.0200 deg.
Attachment	None	Scan axis	2Theta/Theta
Filter	Cu_K-beta	Scan range	20.0000–90.0000 deg.
CBO selection slit	None	Incident slit	2/3 deg
Diffracted beam mono.	None	Length limiting slit	None
Detector	D/teX Ultra	Receiving slit #1	4.000 deg
Scan mode	Continuous	Receiving slit #2	13.000 mm

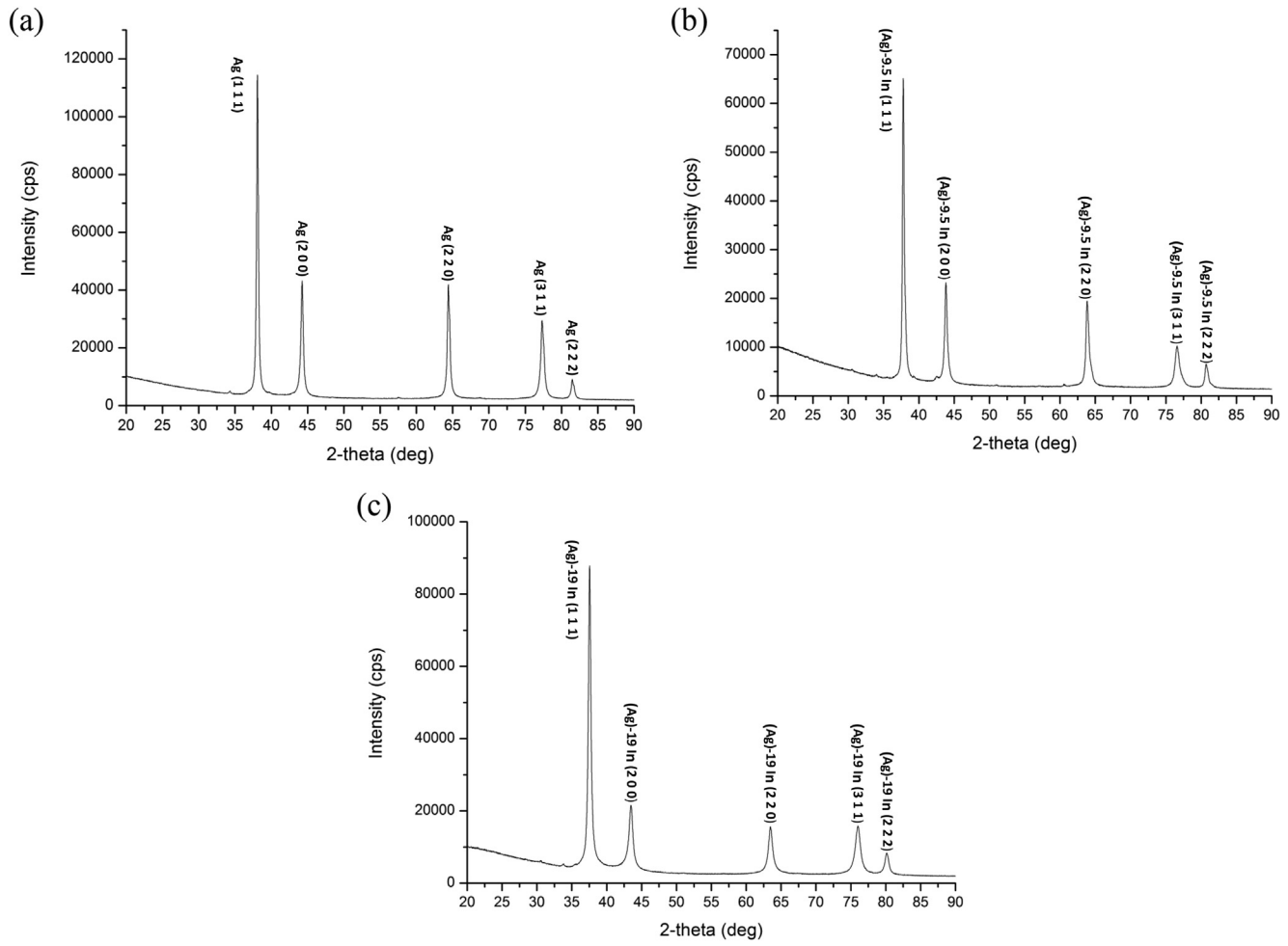

Fig. 3. (a) XRD pattern of pure silver disk sample, (b) XRD pattern of (Ag)–9.5In disk sample, (c) XRD pattern of (Ag)–19In disk sample.

Table 3
(a) A summary of XRD measurement data of pure silver disk sample after PDXL analysis, (b) A summary of XRD measurement data of (Ag)–9.5In disk sample after PDXL analysis, (c) A summary of XRD measurement data of (Ag)–19In disk sample after PDXL analysis.

(a)				
Peaks #	2θ (deg)	d (Å)	(h, k, l)	a (Å)
1	38.082	2.365	(1 1 1)	4.096
2	44.231	2.048	(2 0 0)	4.096
3	64.378	1.447	(2 2 0)	4.093
4	77.324	1.234	(3 1 1)	4.093
5	81.485	1.181	(2 2 2)	4.091
(b)				
Peaks #	2θ (deg)	d (Å)	(h, k, l)	a (Å)
1	37.769	2.380	(1 1 1)	4.122
2	43.825	2.067	(2 0 0)	4.134
3	63.816	1.457	(2 2 0)	4.121
4	76.572	1.244	(3 1 1)	4.126
5	80.679	1.191	(2 2 2)	4.126
(c)				
Peaks #	2θ (deg)	d (Å)	(h, k, l)	a (Å)
1	37.531	2.394	(1 1 1)	4.147
2	43.474	2.082	(2 0 0)	4.164
3	63.423	1.467	(2 2 0)	4.149
4	75.947	1.253	(3 1 1)	4.156
5	80.179	1.197	(2 2 2)	4.147

performed by EDM outsource company. In Fig. 4 and Table 4, the geometry and dimensions of the tensile test sample are shown respectively. EDM machining can change the surface properties of the work piece, causing the issues such as recasting, heat affected zone (HAZ) grain size enlargement. Therefore, all of the obtained tensile test samples were polished using silicon carbide abrasive papers with 800 grits to remove the HAZ layer on the surface of the tensile test samples. Next, the tensile test samples were put into an oven, annealing at 223 °C (homologous temperature $T_h = 0.5$) for 1 h, in order to release the residue internal stress induced by the polishing process. After the preparation, all of the tensile test samples were examined using XRD approach that mentioned previously with the same setting. By comparing the XRD patterns with previous results, the authors can confirm that the tensile test samples have the same composition as the previous disk samples.

The tensile test is performed using the facility, INSTRON 5500R tensile tester, with the deformation rate of 10^{-4} mm/s at controlled

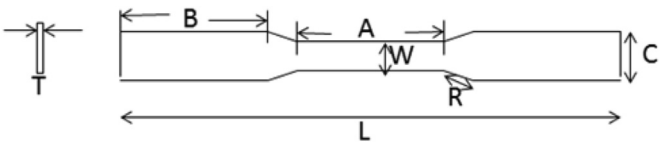

Fig. 4. The geometry of tensile test sample, in accordance with ASTM standard E8/E8M- 08.

Table 4
The dimensions of tensile test sample, in accordance with ASTM standard E8/E8M-08.

Unit	W	T	R	L	A	B	C
mm	2.00	1.10	2.00	33.33	10.67	10.00	3.30
inch	0.08	0.04	0.08	1.31	0.42	0.39	0.13

software panel setting. Since the real tensile test samples sizes may vary a little bit from its original design, all of the critical dimensions such as the length of the tested region, A, width of the tested region, W, and the thickness of the sample, T, need to be measured and calibrate at the control software panel. Therefore, the true strain rate is in the vicinity of 10^{-5}/s, which is under the condition of static tension test. During tensile test, the sample is under uniaxial tensile stress initially since the shape of the sample is longitudinal symmetric. The data of engineering stress and strain is recorded, collected, and calculated automatically by the controlled software. (Ag)–9.5In and (Ag)–19In tensile samples were tested with the reference of pure Ag samples in comparison.

4. Stress vs. strain characterization

The true stress and strain can be calculated using the Eqs. (1) and (2) [16]:

$$\sigma = s(e+1) \tag{1}$$

$$\varepsilon = ln(e+1) \tag{2}$$

where s is the engineering stress, e is the engineering strain, σ is the true stress, and ε is the true strain.

Due to the limitation of the casting method, the ingots may have some defects inside such as cavities and cracks in micron range. In addition, the tensile test samples are from the different locations of the ingots, so that the major orientation of the grains or texture in the each tensile test samples may vary from one to another, and this also applies to the distribution of cavity and cracks in each sample. In Fig. 5, three representative results of tensile test for pure Ag, (Ag)–9.5In, and (Ag)–19In are plotted for their engineering stress vs. strain curves. Using the equations (1) and (2) given above, true stress and strain can be calculated for each data point, thereby plotting true stress vs. strain curves correspondingly, as shown in Fig. 6. Mechanical properties of silver–indium solid solution, especially for materials properties of plasticity, such as yield strength, ultimate tensile strength (UTS), true uniform strain and true fracture strain in tension stress status, can be characterized, using the obtained true stress–strain curves. The values of these mechanical properties are summarized and documented in Table 5.

Typically, as predicted in solid solution strengthening theory, the usual result of solute additions is to raise the yield stress and the level of the stress–strain curve as a whole [16]. However, as shown in Table 5, the observation based on the tensile test experiment in silver–indium solid solution system is abnormal to solid solution strengthening theory. The tensile test samples should have similar microstructures due to the fact that the annealing profiles of the ingots growth are similar to each other. Therefore, the major variable here is the solute composition difference. With 9.5 at.% indium element alloying element addition, the yield strength drops from 56 MPa for pure silver to 37 MPa for 9.5 at.% silver indium solid solution, but it increases back to 53 MPa for 19 at.% indium element alloying. This phenomenon can be referred to as solid solution softening theory [17]. According to the reference, solid solution hardening and softening can both occur in the same alloying system depending on several factors such as temperature, solute atom concentration, etc. The solid solution softening mechanism usually occur in substitutional alloy when solute atoms concentrations are relatively high where random distribution of solute atoms would be not be expected. The softening additions are found to locally change the chemical bonding which results in a decrease of the generalized stacking fault energy and atomic row shear resistance with the enhancement of double kink nucleation and dislocation mobility, thereby decreasing the hardness and yield stress of the material. Solid solution softening couples can be commonly found in iron and molybdenum body-centered cubic (BCC) alloying systems [18]. With alloying with high indium solute concentration in silver solid solution, the occurrence of lower yield stress observed in (Ag)–xxIn phase can be partially explained by the solid solution softening theory. However, further research may be needed to investigate the reason behind the increment of yield strength from 9.5 at.% to 19 at.% of indium.

As shown in Fig. 6, the shape of the onset of yielding in the stress vs. strain curves of pure Ag and (Ag)–9.5In are similar which both have gradual transition from elastic region to plastic region. The strain hardening rate of pure silver and (Ag)–9.5In are almost

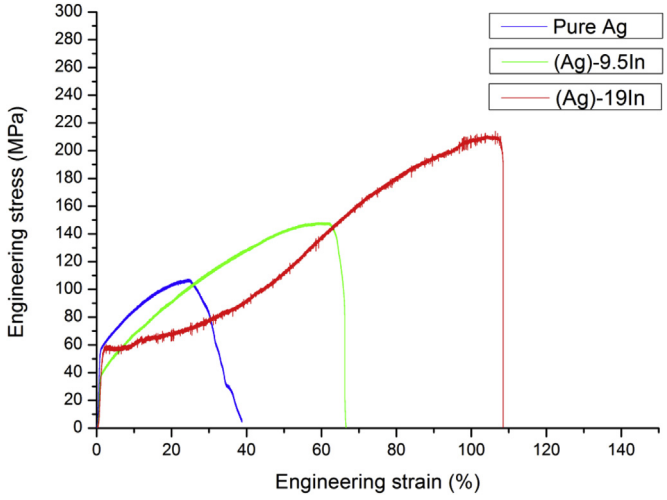

Fig. 5. (a) The engineering stress–strain curve of pure silver, (b) The engineering stress–strain curve of (Ag)–9.5In, (c) The engineering stress–strain curve of (Ag)–19In.

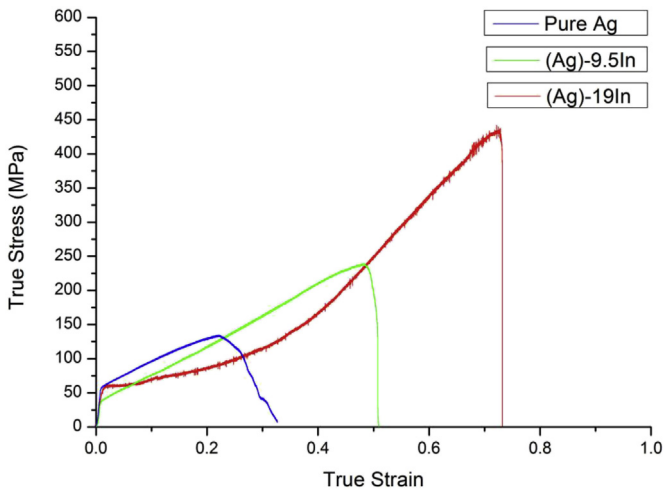

Fig. 6. (a) The true stress–strain curve of pure silver, (b) The true stress–strain curve of (Ag)–9.5In, (c) The true stress–strain curve of (Ag)–19In.

Table 5
A summary of mechanical properties of (Ag)–9.5In and (Ag)–19In with pure Ag in comparison.

	Yield strength (MPa)	Ultimate tensile strength (MPa)	True uniform strain (%)	True fracture strain (%)
Pure Ag	56.6	133.9	22.0	32.7
(Ag)–9.5In	37.2	240.1	48.3	50.9
(Ag)–19In	53.2	447.5	72.5	73.4

constant due to the fact that these two curves have linear shape from yield point to UTS point. As listed in Table 5, the ultimate tensile strength, true uniform strain (strain upon UTS point), and true fracture strain (strain upon fracture point) are increased with 9.5 at.% indium element addition. In other words, the strength and the ductility of the material are simultaneously increased by adding solid solution solute, which usually can be only accomplished by decreasing of the grain size.

However, the shape of stress vs. strain curve of (Ag)–19In has major differences, comparing with that of pure Ag and (Ag)–9.5In. The transition from elastic region to plastic region is quite sharp, followed by a plateau plastic deformation region with relatively low strain hardening rate. The strain hardening rate gradually increases as the material continues to plastically deform, reaching its maximum value at point where true strain equals to 0.45, and then remains to constant value until the material fractures. It is worthwhile to note that the ultimate tensile strength, true uniform, and true fracture strain are much higher than that of pure Ag and (Ag)–9.5In. Base on the information provided by the stress vs. strain curves, it is safe to conclude that both mechanical strength and ductility will increase as the indium alloying element concentration increases in silver solid solution phase.

5. Fractography

As shown in Fig. 5, the engineering strain of (Ag)–19In at fracture point, i.e., the material elongation is more than 100%, which means it exhibits excellent ductility. To the best knowledge of the authors, the silver and its alloys' elongation usually are within the range from 35% to 50%. Therefore, the high elongation value of silver indium solid solution with high indium concentration is truly remarkable.

In order to confirm the mechanism of deformation and failure mode of (Ag)–19In, the fracture surface morphology of the same tested sample used to plot Figs. 5 and 6 curves is examined by using SEM to gain some insights of its microscopic nature. In addition, the fracture surface morphology of the same tested samples for Ag and (Ag)–9.5In used to plot Figs. 5 and 6 are shown in Figs. 7 and 8 to compare with the fractography of the (Ag)–19In sample.

As shown in Fig. 9, the surface of fracture is examined at different magnification, and the SEM pictures are shown in a series. A feature of band-like rupture can be clearly seen in these pictures, which means the material has undergone significant plastic deformation before failure. As shown in Fig. 10, a representative dimpled rupture can also be easily observed on the fracture surface. This type of fracture surface denotes a ductile mode fracture. Microvoid formation and coalescence during the continued straining and plastic deformation are responsible for this dimpled rupture fractography [19]. Therefore, it can be safely confirmed that (Ag)–19In is truly ductile in its nature from the study of fractography.

In comparison, as shown in Figs. 7 and 8, the fractography of Ag and (Ag)–9.5In tensile tested samples are different from the one of (Ag)–19In. The authors can only observe shallow dimpled rupture on the fracture surface of Ag sample, whereas the dimpled rupture of (Ag)–19In shown in Fig. 10 is much clearer than that of Fig. 7, thereby confirming (Ag)–19In has undergone much more amounts of plastic deformation upon failure than pure Ag tensile test sample. As shown in Fig. 8, the authors can observe clear dimpled rupture for (Ag)–9.5In tensile tested sample, but band-like rupture is relatively shallow, comparing with that of (Ag)–19In. Therefore, (Ag)–9.5In is more ductile than pure Ag, but not as ductile as (Ag)–19In.

In conclusion, the result of fractography study is in agreement with previous tensile test data, thereby confirming that the ductility will increase as the indium alloying element concentration increases in silver solid solution phase.

6. Conclusion

In the paper, the materials of silver indium solid solution phase have been grown in the ingot form at two different compositions, (Ag)–9.5In and (Ag)–19In, and characterized by XRD and SEM/EDX

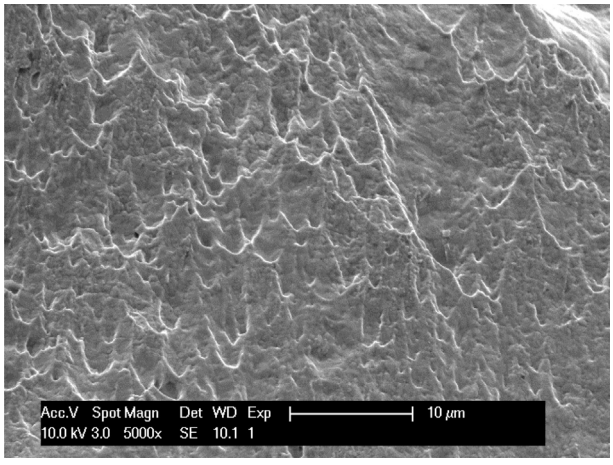

Fig. 7. Fractography of Ag tensile test sample, SEM image at 5000× magnification.

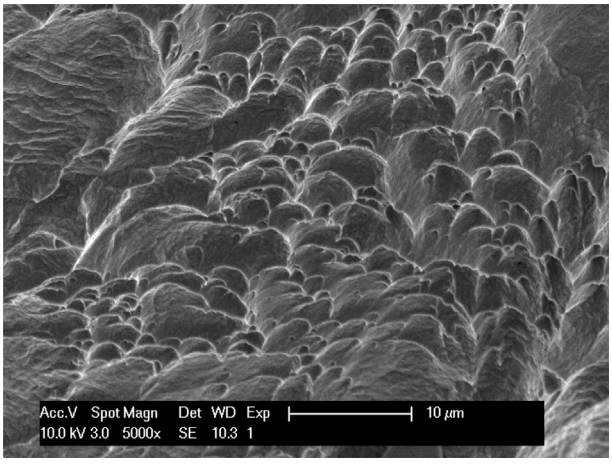

Fig. 8. Fractography of (Ag)–9.5In tensile test sample, SEM image at 5000× magnification.

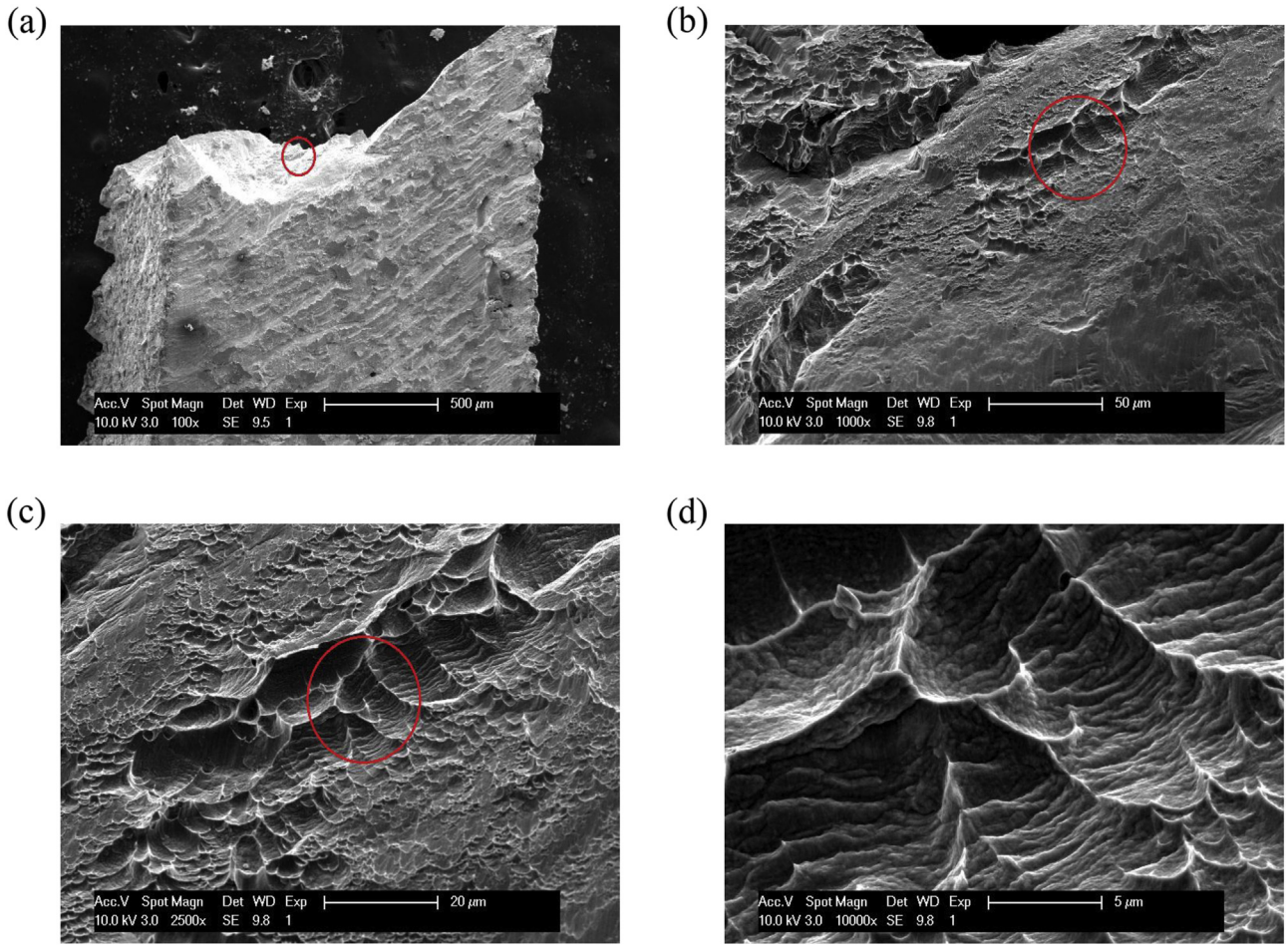

Fig. 9. (a) Fractography of (Ag)–19In tensile test sample, SEM image at 100× magnification, (b) SEM image at 1000× magnification, (c) SEM image at 2500× magnification, (d) SEM image at 10000× magnification.

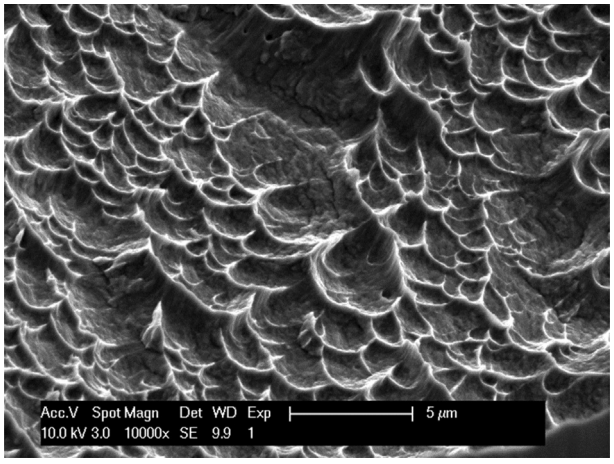

Fig. 10. Representative morphology of dimpled rupture on the fracture surface of (Ag)–19In tensile test sample.

methods. Furthermore, the intrinsic mechanical properties of silver solid solution phase with indium, i.e., the stress vs. strain curves, have been presented and analyzed. Due to the large indium alloying concentration, the phenomenon of solid solution softening has been observed. As a result, the yield stress of the silver indium solid solution phase at two different composition, (Ag)–9.5In and (Ag)–19In, are lower than that of pure silver. In addition, the silver indium solid solution phase exhibits superior ductility, especially for (Ag)–19In, since the its ultimate tensile strength is 3.3 times of that of pure silver, and its elongation upon fracture are 2.2 times of that of pure silver. With the preliminary study of the mechanical properties, the silver indium solid solution phase is a promising candidate for interconnection applications in electronic industries. As interconnection medium, the lower hardness and yield stress would be desirable [20] since it induce less internal stress to the die or bonding pad underneath. With the superior ductility, forming of silver indium solid solution phase is better than that of pure silver, so that it is suitable for being forged into various forms of industrial products. The documentation of the stress vs. strain curves of silver indium solid solution phase would be valuable for further research and investigation for this material. For example, mechanical finite element analysis (FEA) [21,22] regarding to silver indium solid solution phase can be readily performed with the availability of this material mechanical properties such as yield stress, UTS, and stress vs. strain curves. Further work may be continued to study the other interesting properties of silver solid solution phase with indium.

Acknowledgment

The authors would like to express our gratitude towards II-VI Foundation with Grant No. II-VI-104447 for its financial support during our academic research and to thank Dr. Shou-Jen Hsu for his

assistance in setting up the hydrogen torch.

References

[1] W. Hume-Rothery, G.F. Lewin, P.W. Reynolds, The lattice spacings of certain primary solid solutions in silver and copper, Proc. R. Soc. Lond. Ser. A Math. Phys. Sci. 157 (890) (Oct 1936) 0167–0183.

[2] R. Bacon, C.S. Smith, Single crystal elastic constants of silver and silver alloys, Acta Metall. 4 (4) (1956) 337–341.

[3] R.W.K. Honeycombe, The Plastic Deformation of Metals, first ed., Edward Arnold Ltd., Cambridge, 1968.

[4] P. Jax, P. Kratochvil, P. Haasen, Solid solution hardening of gold and other fcc single crystals, Acta Metall. 18 (2) (1970) 237–245.

[5] C.B. Alcock, K.T. Jacob, T. Palamutcu, Thermodynamics of α-solid solutions of silver with indium and tin, Acta Metall. 21 (7) (1973) 1003–1009.

[6] H. Suga, T. Imura, Solid solution hardening of silver single crystals by indium, by tin and by antimony, Jpn. J. Appl. Phys. 14 (8) (1975) 1253–1254.

[7] T.H. Chuang, C.H. Tsai, H.C. Wang, C.C. Chang, C.H. Chuang, J.D. Lee, H.H. Tsai, Effects of annealing twins on the grain growth and mechanical properties of Ag-8Au-3Pd bonding wires, J. Electron. Mater. 41 (11) (2012) 3215–3222.

[8] T.H. Chuang, H.C. Wang, C.H. Chuang, H.J. Lin, J.D. Lee, H.H. Tsai, Surface reconstruction of an annealing twinned Ag-8Au-3Pd alloy wire under current stressing, Metall. Mater. Trans. A 44 (11) (2013) 5106–5112.

[9] Y.C. Chen, W.W. So, C.C. Lee, A fluxless bonding technology using indium-silver multilayer composites, Compon. Packag. Manuf. Technol. A IEEE Trans. 20 (1) (1997) 46–51.

[10] Y.Y. Wu, W.P. Lin, C.C. Lee, A study of chemical reactions of silver and indium at 180 °C, J. Mater. Sci. Mater. Electron. 23 (12) (2012) 2235–2244.

[11] Y.Y. Wu, C.C. Lee, The strength of high-temperature Ag–In joints produced between copper by fluxless low-temperature processes, J. Electron. Packag. 136 (1) (March 2014) 0110061–0110066.

[12] Y. Huo, C.C. Lee, Anti-tarnishing evaluations of silver solid solution phase with indium, in: Electronic Components and Technology Conference (ECTC), 2015 IEEE 65th, IEEE, 2015, pp. 2180–2187.

[13] M.R. Baren, in: C.E.T. White, H. Okamoto (Eds.), Indium Alloys and their Engineering Applications, ASM Intl, Materials Park, OH, 1993, p. 15.

[14] A.N. Campbell, R. Wagemann, R.B. Ferguson, The silver-indium system: thermal analysis, photomicrography, electron microprobe, and X-ray powder diffraction results, Can. J. Chem. 48 (11) (1970) 1703–1715.

[15] ASTM standard E8/E8M- 08, Standard Test Methods for Tension Testing of Metallic Materials, ASTM International, West Conshohocken, PA, 2008, http://dx.doi.org/10.1520/E0008_E0008M-08. www.astm.org.

[16] G.E. Dieter, Mechanical Metallurgy, third ed., Mc Graw Hill, NY, 1986.

[17] A. Sato, M. Meshii, Solid solution softening and solid solution hardening, Acta Metall. 21 (6) (1973) 753–768.

[18] N.I. Medvedeva, Y.N. Gornostyrev, A.J. Freeman, Solid solution softening in bcc Mo alloys: effect of transition-metal additions on dislocation structure and mobility, Phys. Rev. B 72 (13) (2005) 134107.

[19] R.H. Van Stone, T.B. Cox, J.R. Low Jr., J.A. Psioda, Microstructural aspects of fracture by dimpled rupture, Int. Met. Rev. 30 (1) (1985) 157–179.

[20] Z.W. Zhong, H.M. Ho, Y.C. Tan, W.C. Tan, H.M. Goh, B.H. Toh, J. Tan, Study of factors affecting the hardness of ball bonds in copper wire bonding, Microelectron. Eng. 84 (2) (2007) 368–374.

[21] S. Elangovan, S. Semeer, K. Prakasan, Temperature and stress distribution in ultrasonic metal welding – an FEA-based study, J. Mater. Process. Technol. 209 (3) (2009) 1143–1150.

[22] B.H. Ng, A.A.O. Tay, S.H. Ong, Three dimensional finite element simulation of wire looping process in wirebonding, in: Electronics Packaging Technology Conference, 2002. 4th. IEEE, 2002, pp. 334–337.